New Mass-Transfer Model for Simulating Industrial Nylon-6 Production Trains

Kevin C. Seavey, Y. A. Liu,* Bruce Lucas, Neeraj P. Khare, Tom Lee, and Jason Pettrey

Honeywell Center of Excellence in Computer-Aided Design and SINOPEC/FPCC/AspenTech Center of Excellence in Process Systems Engineering, Department of Chemical Engineering, Virginia Polytechnic Institute and State University, Blacksburg, Virginia 24061

Thomas N. Williams, John Mattson, Earl Schoenborn, Charles Larkin, and Harry Hu

Honeywell International, Inc., 15801 Woods Edge Road, Colonial Heights, Virginia 23834

Chau-Chyun Chen

Aspen Technology, Inc., Ten Canal Park, Cambridge, Massachusetts 02141

We present a new mass-transfer model for simulating industrial nylon-6 polymerization trains. In this model, both diffusion and boiling (bubble nucleation) contribute to mass transfer. With this model, we are able to simulate widely differing production technologies using identical mass-transfer parameters, along with identical models for fundamentals such as phase equilibrium, physical properties, and polymerization kinetics. To illustrate, we simulate the direct-melt process and the bubble-gas kettle process. The direct-melt process builds up the polymer molecular weight and removes nearly all residual caprolactam monomer by employing, under vacuum, a wiped-wall evaporator and a rotating-disk finisher. The bubble-gas kettle process, on the other hand, injects inert gas bubbles through the melt at nearly atmospheric pressure to build up the polymer molecular weight but does not significantly reduce the caprolactam level because the diffusion coefficient is so low. We validate our process models using commercial train performance data at different production rates, including the first known validation of a dynamic rate-change simulation for industrial polycondensation trains. Model predictions quantitatively agree with product quality data such as formic acid viscosity (FAV), polymer end-group concentration, and water extractables. The prediction errors for the direct-melt process are 2.81%, −3.13%, and −3.06% for FAV, water extractables, and amine end groups, respectively. For the bubble-gas kettle process, the prediction errors are −17.2%, −17.0%, and −7.49% for extrusion FAV, washed-and-dried FAV, and water extractables, respectively. These errors are much lower than the ca. −50% errors obtained by existing advanced models for devolatilization.

1. Introduction

Engineers use process models to investigate polymerization options. These investigations typically show how output variables, such as the production rate and polymer molecular weight, depend on input variables, such as the reactor temperature, pressure, and residence time. Doing this with a validated simulation model is quicker and cheaper than actually making changes in the plant, especially when the model accurately describes the way the process performs.

When we build process models, we try to employ fundamentals rather than empiricisms. We do so for two reasons: (1) fundamental models oftentimes extrapolate better than empiricisms and (2) fundamental models are oftentimes better able to describe processes at widely differing conditions such as temperature and pressure. These performance advantages, however, do come at a price: we frequently must invest more resources up-front to characterize and understand fundamental mechanisms. However, once we have done this, we can use the model to predict the behavior of other processes without having to tune the model parameters to match data on a case-by-case basis.

Very few have been able to develop predictive and quantitative models for industrial polymerization trains that consist of multiple reactors, separators, evaporators, and finishers, as well as stream recycle. We usually have to fit data to produce a quantitative model, even if models describe two trains of the same design. However, by fitting of data, the predictive aspect is lost. In this work on nylon-6 process modeling, we show that both predictive and quantitative modeling is possible by an integrated application of molecular thermodynamics, transport phenomena, polymerization kinetics, and computer-aided design. We do so using a new mass-transfer model that describes both diffusion and boiling (bubble nucleation), along with fundamental models that represent physical properties, vapor−liquid equilibrium, and polymerization kinetics.

The diffusion contribution of the mass-transfer model has no free parameters. The boiling contribution has two free parameters that we determine using a snapshot of a nylon-6 direct-melt train. By snapshot, we mean information at a given point in time detailing feed conditions, reactor conditions, and product characteristics.

* To whom correspondence should be addressed. Tel.: (540) 231-7800. Fax: (540) 231-5022. E-mail: design@vt.edu.

10.1021/ie040067l CCC: $27.50 © 2004 American Chemical Society
Published on Web 07/03/2004

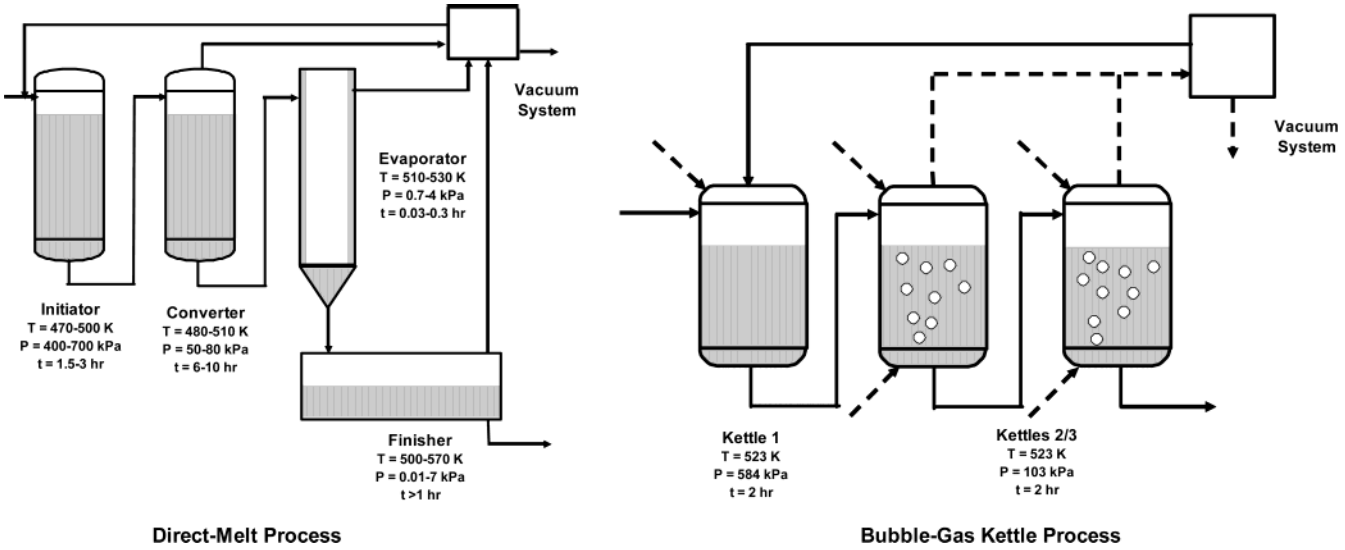

Figure 1. Nylon-6 direct-melt[1,2] and bubble-gas kettle[3] processes.

After we fix the two free parameters, we predict polymer properties at different production rates for both the direct-melt process and the bubble-gas kettle process. In both applications, we compare not only our predictions with plant data but also predictions when other devolatilization models are used, such as a pure-diffusion model and a phase-equilibrium model (i.e., no mass-transfer limitations).

We organize the remainder of this paper as follows. Section 2 gives descriptions for the direct-melt process and the bubble-gas kettle process. Section 3 discusses fundamentals, including kinetics, phase equilibrium, physical properties, and mass transfer. Section 4 presents model validations for both processes over a range of production rates. This section also compares our model predictions with other theories for mass transfer in polycondensation reactors. Section 5 illustrates an application of our mass-transfer model in which we simulate and validate a dynamic rate change for a direct-melt train. We know of no other dynamic modeling and validation studies in the industrial polycondensation literature. Section 6 summarizes the conclusions.

2. Industrial Nylon-6 Polymerization Processes

This paper discusses the modeling of two very different processes, the direct-melt process and the bubble-gas kettle process.

2.1. Direct-Melt Process. The direct-melt process has the highest production capacity, sometimes producing nylon-6 at rates exceeding 10 000 kg/h. Figure 1 shows the flowchart for a direct-melt process together with the typical operating temperature, pressure, and residence time.[1]

The following process information comes from ref 1. The reactor feed typically contains fresh caprolactam monomer, recycled monomer, water, polycondensation catalyst, and chain-terminating agents such as monofunctional acids and amines. These agents improve the dyeing characteristics of spun nylon-6 polymer and limit molecular-weight growth in the evaporator and finisher.

The initiator and converter, collectively named *the front end*, convert monomer into polymer. Typical per-pass conversion is 85%. The evaporator and finisher, collectively named *the back end*, remove water and water extractables, such as monomer and linear/cyclic oligomers. The back end also builds up the polymer molecular weight. The finisher product is a polymer that we can directly extrude into fibers; i.e., we do not have to pelletize it, leach it, and dry it. Volatilized monomer is recovered and recycled by the vacuum system, which condenses the monomer and separates it from water vapor.

Elevated pressure in the initiator keeps water in the liquid phase. This promotes the ring opening of caprolactam. A moderate vacuum in the converter removes most of the water and some of the monomer. A high vacuum in the evaporator and finisher completes the removal of water and water extractables and thereby promotes polycondensation and molecular-weight build-up. All of the reactors are plug-flow-like.

2.2. Bubble-Gas Kettle Process. The bubble-gas kettle process can produce unterminated polymer with a molecular weight exceeding 20 000.[3,4] The drawback is that it does not remove a significant portion of water extractables. The polymer contains about 12% water extractables,[3] and we must pelletize, leach, and dry it to obtain nearly pure product. What we get in return is enhanced reliability because we are not using a vacuum. Figure 1 shows the flowchart for a typical bubble-gas kettle process.[3]

Reference 3 gives the following general information about the bubble-gas kettle process. Caprolactam monomer, steam, and recycled monomer enter the first kettle. This process does not typically employ polycondensation catalysts or terminators.

The steam feed creates a high pressure in the first kettle and promotes conversion by forcing water into the liquid phase. The second and third kettles promote devolatilization by exposing the polymer to vapor phases. These vapor phases, containing steam and/or inert gas, are either swept over or forced (bubbled) through the polymer. The vapor exit stream contains inert gas, steam, and caprolactam and goes to monomer recovery. The recovered monomer is recycled back to the first kettle.

There are two differences between this train and the direct-melt train. The first concerns pressure: back-end bubble-gas kettles operate at 103 000 Pa, while back-end direct-melt reactors operate at 10−7000 Pa. The second concerns the way that reactors devolatilize melts: bubble-gas kettles use forced and sweep vapor streams, while direct-melt reactors use vacuum and

complicated reactor internals to generate the interfacial surface area.

3. Model Development

We now discuss how we model both the direct-melt process and the bubble-gas kettle process. We include three key, fundamental aspects, which are (1) reaction kinetics, (2) phase equilibrium and physical properties, and (3) mass-transfer-limited devolatilization.

We have previously reported on a segment-based approach for expressing nylon-6 polymerizations with acetic acid.[5] In that same work,[5] we also detail the POLYNRTL activity-coefficient model. Other researchers, including Laubriet et al.[6] and Woo et al.,[7−9] have presented work on modeling diffusion in rotating-disk reactors and forced-gas kettles. Therefore, we only present the pertinent equations and point the reader to references detailing their development. We devote a separate section for our new development, which is the application of bubble-nucleation theory to further refine our model of devolatilization in nylon-6 reactors.

3.1. Reaction Kinetics, Phase Equilibrium, and Diffusion. We consider small molecules and polymer. The small molecules are water (W), caprolactam (CL), cyclic dimer (CD), aminocaproic acid (ACA), acetic acid (AA), and cyclohexylamine (CHA). AA and CHA are monofunctional terminators. Please refer to Seavey et al.[5] for a description of the segment methodology[10] that we employ. Note that we do not use the moment approach that is detailed in textbooks such as work by Gupta and Kumar[11] because these equations are cumbersome to derive for multiple terminators. Table 1 shows the reactions in segment notation, along with corresponding rate expressions. It also summarizes the species balance equations due to reaction terms only. To compute the rate constants k_1-k_5, we use parameters similar to those of Arai et al.[12] These parameters, along with the equations, accurately represent all literature data and 250% more additional in-house polymerization data covering the temperature and composition ranges encountered in our industrial processes.

We compute the number-average degree of polymerization DP_n using the following formula:

$$DP_n = \frac{[\text{B-ACA}] + [\text{T-COOH}] + [\text{T-NH}_2]}{[\text{T-NH}_2] + [\text{T-AA}]} \quad (1)$$

The key product output variables are formic acid viscosity (FAV), water extractables, and end-group concentrations. The FAV is the ratio between the viscosities of a nylon-6 solution in formic acid and pure formic acid.[13] There are two types of FAV that we consider. The first is the *washed-and-dried* FAV (W&D FAV), which is the FAV measured on a leached and dried polymer sample. The second is an *extrusion* FAV, which is the FAV measured on an unleached sample. We predict the W&D FAV using an in-house correlation with the number-average molecular weight. An example of a similar correlation appears in the report of Akkapeddi et al.:[4]

$$FAV = 9.38 \times 10^{-9} MW_w^{2.15} \quad (2)$$

This correlation uses MW_w, the weight-average molecular weight. We predict the extrusion FAV using another in-house correlation with the W&D FAV and the level of water extractables.

We compute the water extractables (mass %) by first considering the concentrations of the small molecules (water, caprolactam, cyclic dimer, aminocaproic acid, acetic acid, and cyclohexylamine). We then use an in-house correlation to account for the presence of oligomers of length three through seven. These oligomers, plus the caprolactam and cyclic dimer, approximate the concentration of water extractables.

Since we track all segment concentrations, the amine and carboxylic acid end-group concentrations (mmol/kg) are simply equal to the concentrations of $T\text{-}NH_2$ and T-COOH, respectively.

We do not compute the weight-average or higher averages of the molecular-weight distribution. We do not need the higher molecular weight averages to estimate the key product output variables.

We use the property method of Seavey et al.[5] to describe phase equilibrium and physical properties. Table 1 gives the parameters and equations necessary to compute vapor pressure, molar volume and density, and binary interaction parameters.

We use penetration theory[11,17] to describe diffusion on a macroscopic scale (Laubriet et al.[6]). Other notable researchers who have modeled diffusion on a macroscopic scale are Ravindranath and Mashelkar,[18] Gupta et al.,[19,20] and Wajge et al.[21] Ault and Mellichamp,[22] Gupta et al.,[23] Amon and Denson,[24] and Ahn[25] previously modeled diffusion on a microscopic scale. We estimate the mass-transfer parameter for wiped-wall and rotating-disk reactors using geometric expressions from Ravetkar and Kale.[26] For forced-gas kettles, we use the equations developed by Woo et al.[7−9] to describe bubble dynamics, namely, the size and residence time of injected gas bubbles.

We estimate the diffusion coefficients of caprolactam and water using data. Nagasubramanian and Reimschuessel[27] report the diffusion coefficient of caprolactam at 265 °C and a ∼10/90% (w/w) caprolactam/nylon-6 solution containing a small amount of water. Bonifaci and Ravanetti[28] also present the diffusion coefficient of caprolactam within a temperature range of 250−280 °C and at ∼100% nylon-6. We use the Bonifaci and Ravanetti data[28] to obtain the activation energy for diffusion and the Nagasubramanian and Reimschuessel data[27] to obtain the preexponential factor. Our final expression is

$$\mathscr{D}_{CL} = 1.41 \times 10^{-8}\ (\text{m}^2/\text{s}) \exp\left(-\frac{33457\ (\text{J/mol})}{RT}\right) \quad (3)$$

Nagasubramanian and Reimschuessel[27] also measure the diffusion coefficient of water at 265 °C; however, to our knowledge, there are no other data for the diffusion of water under polymerization conditions. We therefore approximate the activation energy of diffusion for water using its self-diffusion coefficient. This is the best available estimate of the activation energy.[29]

To estimate the self-diffusion coefficient, we use the Dullien equation[30] and the physical property parameters for water in work by Daubert and Danner:[15]

$$\mathscr{D}_{i,\text{self}} = D_{0,i} \exp\left(-\frac{E_{a,i}}{RT}\right) = \frac{(0.124 \times 10^{-16}\ \text{mol}^{2/3})\tilde{V}_{c,i}^{2/3} RT}{\mu_i \hat{V}_i^0 M_i} \quad (4)$$

Table 1. Reaction Kinetics, Phase Equilibrium, Physical Property, and Diffusion Models Employed in This Study

Reactions	
equilibrium reaction	reaction rate
Ring Opening of Caprolactam ($W + CL \underset{k_1'}{\overset{k_1}{\rightleftharpoons}} ACA$)	
$CL + W \underset{k_1'=k_1/K_1}{\overset{k_1}{\rightleftharpoons}} ACA$	$R_1 = k_1[CL][W] - k_1'[ACA]$
Polycondensation ($P_n + P_m \underset{k_2}{\overset{k_2'}{\rightleftharpoons}} P_{n+m} + W$)	
$ACA + ACA \underset{k_2'=k_2/K_2}{\overset{k_2}{\rightleftharpoons}} \text{T-COOH/T-NH}_2 + W$	$R_2 = k_2[ACA]^2 - k_2'[W][\text{T-NH}_2]\left(\frac{[\text{T-COOH}]}{[\text{T-COOH}] + [\text{B-ACA}] + [\text{T-CHA}]}\right)$
$ACA + \text{T-COOH} \underset{k_2'=k_2/K_2}{\overset{k_2}{\rightleftharpoons}} \text{T-COOH/B-ACA} + W$	$R_3 = k_2[ACA][\text{T-COOH}] - k_2'[W][\text{T-COOH}]\left(\frac{[\text{B-ACA}]}{[\text{B-ACA}] + [\text{T-NH}_2] + [\text{T-AA}]}\right)$
$\text{T-NH}_2 + ACA \underset{k_2'=k_2/K_2}{\overset{k_2}{\rightleftharpoons}} \text{T-NH}_2\text{/B-ACA} + W$	$R_4 = k_2[\text{T-NH}_2][ACA] - k_2'[W][\text{T-NH}_2]\left(\frac{[\text{B-ACA}]}{[\text{B-ACA}] + [\text{T-COOH}] + [\text{T-CHA}]}\right)$
$\text{T-NH}_2 + \text{T-COOH} \underset{k_2'=k_2/K_2}{\overset{k_2}{\rightleftharpoons}} \text{B-ACA/B-ACA} + W$	$R_5 = k_2[\text{T-NH}_2][\text{T-COOH}] - k_2'[W][\text{B-ACA}]\left(\frac{[\text{B-ACA}]}{[\text{B-ACA}] + [\text{T-NH}_2] + [\text{T-AA}]}\right)$
Polyaddition of Caprolactam ($CL + P_n \underset{k_3'}{\overset{k_3}{\rightleftharpoons}} P_{n+1}$)	
$ACA + CL \underset{k_3'=k_3/K_3}{\overset{k_3}{\rightleftharpoons}} \text{T-NH}_2\text{/T-COOH}$	$R_6 = k_3[ACA][CL] - k_3'[\text{T-NH}_2]\left(\frac{[\text{T-COOH}]}{[\text{T-COOH}] + [\text{B-ACA}] + [\text{T-CHA}]}\right)$
$\text{T-NH}_2 + CL \underset{k_3'=k_3/K_3}{\overset{k_3}{\rightleftharpoons}} \text{T-NH}_2\text{/B-ACA}$	$R_7 = k_3[\text{T-NH}_2][CL] - k_3'[\text{T-NH}_2]\left(\frac{[\text{B-ACA}]}{[\text{B-ACA}] + [\text{T-COOH}] + [\text{T-CHA}]}\right)$
Ring Opening of a Cyclic Dimer ($W + CD \underset{k_4'}{\overset{k_4}{\rightleftharpoons}} P_2$)	
$CD + W \underset{k_4'=k_4/K_4}{\overset{k_4}{\rightleftharpoons}} \text{T-COOH/T-NH}_2$	$R_8 = k_4[CD][W] - k_4'[\text{T-NH}_2]\left(\frac{[\text{T-COOH}]}{[\text{T-COOH}] + [\text{B-ACA}] + [\text{T-CHA}]}\right)$
Polyaddition of a Cyclic Dimer ($CD + P_n \underset{k_5'}{\overset{k_5}{\rightleftharpoons}} P_{n+2}$)	
$ACA + CD \underset{k_5'=k_5/K_5}{\overset{k_5}{\rightleftharpoons}} \text{T-NH}_2\text{/B-ACA/T-COOH}$	$R_9 = k_5[ACA][CD] - k_5'[\text{T-NH}_2]\left(\frac{[\text{B-ACA}]}{[\text{B-ACA}] + [\text{T-COOH}] + [\text{T-CHA}]}\right) \times \left(\frac{[\text{T-COOH}]}{[\text{B-ACA}] + [\text{T-COOH}] + [\text{T-CHA}]}\right)$
$\text{T-NH}_2 + CD \underset{k_5'=k_5/K_5}{\overset{k_5}{\rightleftharpoons}} \text{B-ACA/B-ACA/T-NH}_2$	$R_{10} = k_5[\text{T-NH}_2][CD] - k_5'[\text{T-NH}_2]\left(\frac{[\text{B-ACA}]}{[\text{B-ACA}] + [\text{T-COOH}] + [\text{T-CHA}]}\right)^2$
Polycondensation of Acetic Acid ($P_n + AA \underset{k_2'}{\overset{k_2}{\rightleftharpoons}} P_{n,\text{T-AA}} + W$)	
$ACA + AA \underset{k_2'=k_2/K_2}{\overset{k_2}{\rightleftharpoons}} \text{T-AA/T-COOH} + W$	$R_{11} = k_2[AA][ACA] - k_2'[W][\text{T-AA}]\left(\frac{[\text{T-COOH}]}{[\text{T-COOH}] + [\text{B-ACA}]}\right)$
$\text{T-NH}_2 + AA \underset{k_2'=k_2/K_2}{\overset{k_2}{\rightleftharpoons}} \text{B-ACA/T-AA} + W$	$R_{12} = k_2[AA][\text{T-NH}_2] - k_2'[W][\text{T-AA}]\left(\frac{[\text{B-ACA}]}{[\text{T-COOH}] + [\text{B-ACA}]}\right)$
Polyaddition of Caprolactam by Cyclohexylamine ($CL + CHA \underset{k_3'}{\overset{k_3}{\rightleftharpoons}} P_{1,\text{T-CHA}}$)	
$CHA + CL \underset{k_3'=k_3/K_3}{\overset{k_3}{\rightleftharpoons}} \text{T-NH}_2\text{/T-CHA}$	$R_{13} = k_3[CHA][CL] - k_3'[\text{T-CHA}]\left(\frac{[\text{T-NH}_2]}{[\text{T-NH}_2] + [\text{B-ACA}]}\right)$
Polycondensation of Cyclohexylamine ($P_n + CHA \underset{k_2'}{\overset{k_2}{\rightleftharpoons}} P_{n,\text{T-CHA}} + W$)	
$CHA + ACA \underset{k_2'=k_2/K_2}{\overset{k_2}{\rightleftharpoons}} \text{T-NH}_2\text{/T-CHA} + W$	$R_{14} = k_2[CHA][ACA] - k_2'[W][\text{T-CHA}]\left(\frac{[\text{T-NH}_2]}{[\text{T-NH}_2] + [\text{B-ACA}]}\right)$
$CHA + \text{T-COOH} \underset{k_2'=k_2/K_2}{\overset{k_2}{\rightleftharpoons}} \text{B-ACA/T-CHA} + W$	$R_{15} = k_2[CHA][\text{T-COOH}] - k_2'[W][\text{T-CHA}]\left(\frac{[\text{B-ACA}]}{[\text{T-NH}_2] + [\text{B-ACA}]}\right)$

Table 1 (Continued)

Rate of Generation Due to Reaction

W	$R_2 + R_3 + R_4 + R_5 + R_{11} + R_{12} + R_{14} + R_{15} - (R_1 + R_8)$
CL	$-(R_1 + R_6 + R_7 + R_{13})$
CD	$-(R_8 + R_9 + R_{10})$
AA	$-(R_{11} + R_{12})$
CHA	$-(R_{13} + R_{14} + R_{15})$
ACA	$R_1 - (2R_2 + R_3 + R_4 + R_6 + R_9 + R_{11} + R_{14})$
B-ACA	$R_3 + R_4 + 2R_5 + R_7 + R_9 + 2R_{10} + R_{12} + R_{15}$
T-NH_2	$R_2 + R_6 + R_8 + R_9 + R_{13} + R_{14} - (R_5 + R_{12})$
T-COOH	$R_2 + R_6 + R_8 + R_9 + R_{11} - (R_5 + R_{15})$
T-AA	$R_{11} + R_{12}$
T-CHA	$R_{13} + R_{14} + R_{15}$

Equilibrium and Physical Properties[14−16]

POLYNRTL binary interaction parameters	$\tau_{ij} = a_{ij} + \frac{b_{ij}}{T} + c_{ij} \ln T$
vapor pressure	$P_i^{sat} = \exp\left(A_i + \frac{B_i}{T} + C_i \ln T + D_i T^{E_i}\right)$
molar volume	$\frac{1}{\nu_i} = \frac{A_i}{B_i^{1+(1-T/C_i)^{Di}}}$
polymer density	$\nu_i = \nu_i(T,0)\left[1 - 0.0894 \ln\left(1 + \frac{P,\ \text{Pa}}{B_i(T)}\right)\right]$, $220\ ^\circ\text{C} < T < 300\ ^\circ\text{C}$
(τ_{ij} = binary interaction parameter, T = temperature, P_i^{sat} = vapor pressure, ν_i = molar volume or density, P = pressure)	$\nu_i(T,0)$, $\text{m}^3/\text{kg} = 9.4650 \times 10^{-4} + (1.2273 \times 10^{-9})(T, ^\circ\text{C})^2$ $B_i(T)$, Pa $= (3.3232 \times 10^8) \exp[(-1)(3.8193 \times 10^{-3})(T, ^\circ\text{C})]$

Equilibrium Parameters[5]

	i = water and j = caprolactam	i = water and j = nylon-6 segment	i = caprolactam and j = nylon-6 segment
a_{ij}	−0.313	0	0
a_{ji}	0.628	0	0
b_{ij}	−15.4	297	265
b_{ji}	−13.7	−601	207
c_{ij}	0.0495	0	0
c_{ji}	−0.0898	0	0

Physical Property Parameters[15]

constant	water	caprolactam
vapor pressure (Pa)		
A_i	7.3649×10^1	7.4172×10^1
B_i (K)	-7.2582×10^3	-1.0469×10^4
C_i	−7.3037	−6.8944
D_i	4.1653×10^{-6}	1.2113×10^{-18}
E_i (K^{-E})	2.0000	6.0000
Liquid molar volume (m^3/kmol)		
A_i (kmol/m^3)	5.4590	7.1180×10^{-1}
B_i	3.0542×10^{-1}	2.5400×10^{-1}
C_i (K)	6.4713×10^2	8.0600×10^2
D_i	8.1000×10^{-2}	2.8570×10^{-1}

Diffusional Mass Transfer[6,11,17]

mass-transfer equation	$E_{i,D} = k_{L,i} A_{int}(C_i - C_{i*})$
mass-transfer coefficient	$k_{L,i} = 2\sqrt{\frac{\mathscr{D}_i}{\pi\theta}}$
($E_{i,D}$ = evaporation rate, $k_{L,i}$ = mass-transfer coefficient, A_{int} = interfacial surface area, C_i = bulk liquid concentration, C_{i*} = interfacial concentration, D_i = diffusion coefficient, θ = contact time)	

Wiped-Film Evaporators and Rotating-Disk Reactors[26]

interfacial area (wiped-film evaporator)	$A_{int} = 2\pi RL$
contact time (wiped-film evaporator)	$\theta = 1/WS$
(A_{int} = interfacial surface area, R = radius of evaporator, L = length of evaporator, θ = contact time, W = number of wipers, S = rotation rate)	
interfacial surface area (rotating-disk reactor)	$A_{int} = 2\pi R^2\left[\frac{(2\pi - \text{angle})}{2\pi} + \frac{\sin(\text{angle})}{2\pi} - \frac{1 + \cos(\text{angle})}{2}\right]$
contact time (rotating-disk reactor)	$\theta = \frac{2\pi - \text{angle}}{2\pi\omega}$
(A_{int} = interfacial surface area, R = radius of disk, angle = angle made by drawing lines from the axis of the reactor to the point where the liquid level touches both the reactor wall and vapor phase, θ = contact time, ω = rotation rate)	

Table 1 (Continued)

Forced-Gas Kettles[7−9]	
bubble diameter	$d_b = 2.313\left(\frac{\mu Q_G}{\rho g}\right)^{0.25}$
bubble rise velocity	$u_b = \left[\frac{2d_b g}{16\mu/\rho u_b d_b + 1}\left(1 + \frac{Q_G d_b}{u_b V_G^*}\right)\right]$
fractional holdup	$\epsilon_G = 0.239(u_b \times 10^{-2})D_R^{-0.5}$
number of bubbles in the liquid	$N_b = \frac{Q_G \theta}{V_G^*}$
interfacial surface area	$A_{int} = 4\pi\left(\frac{d_b}{2}\right)^2 N_b$
contact time	$\theta = \frac{V_L(1+\epsilon_G)}{u_b S_R}$

(d_b = bubble diameter, μ = viscosity, Q_G = volumetric flow rate of the gas, ρ = fluid density, g = gravitational acceleration constant, u_b = bubble rise velocity, V_G^* = bubble volume, ϵ_G = fractional gas holdup, D_R = reactor diameter, A_{int} = interfacial surface area, θ = contact time, V_L = liquid volume, S_R = reactor cross-sectional area)

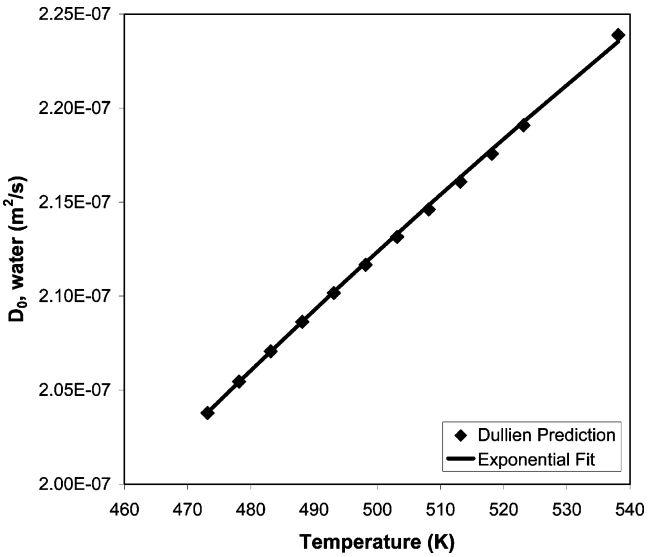

Figure 2. Prediction of the self-diffusion coefficient of water by the Dullien equation, eq 29. The exponential fit describes the proportionality between the self-diffusion coefficient and exp[−3010 (J/mol)/RT].

$\tilde{V}_{c,i}$ is the critical molar volume of the solvent (m^3/mol), and M_i is the molecular weight of the solvent. $\hat{V}_i^0$ is the specific volume of the pure solvent (m^3/kg), and the self-diffusion coefficient $\mathscr{D}_{i,self}$ has units of m^2/s. $D_{0,i}$ is the preexponential factor for the self-diffusion coefficient (m^2/s), and μ_i is the viscosity (Pa s). Figure 2 shows the self-diffusion coefficient predictions.

The activation energy for diffusion is 3010 J/mol. Using this activation energy and the one data point for the water diffusion coefficient at 265 °C to characterize the preexponential factor, we arrive at the following expression for the diffusion coefficient of water in molten nylon-6:

$$\mathscr{D}_W = 2.21 \times 10^{-8}\ (m^2/s)\ \exp\left(-\frac{3010\ (J/mol)}{RT}\right) \quad (5)$$

3.2. Bubble Nucleation. All previous reactor models for step-growth polymerizations [e.g., nylon-6 and poly(ethylene terephthalate) (PET)] only consider diffusion when modeling devolatilization.[11] In particular, all past devolatilization models use either fundamental diffusion equations or mass-transfer equations from penetration theory. We believe that boiling is important because we have visually observed boiling in batch reactors, vacuum finishers, bubble-gas kettles, etc. While we have known that boiling is a contributing mechanism to devolatilization in polyolefin systems,[31−34] no one has considered boiling itself as a mode of devolatilization in step-growth polymerization systems. When we say "no one", we mean although others have treated devolatilization indirectly using empirical mass-transfer coefficients, no one has treated boiling explicitly and fundamentally, i.e., using bubble-nucleation equations.

In 1975, Katz and co-workers published studies quantifying the rate at which bubbles nucleate in pure-component and multicomponent liquids.[35,36] For a mixture, they compute the rate at which bubbles nucleate J:

$$J = A\left(\sum_i \frac{y_i}{\sqrt{M_i}}\right)\exp\left[-\frac{B}{T(P_V - P_L)^2}\right] \quad (6)$$

J is the nucleation rate of bubbles (# s), M_i is the molecular weight of the vaporizing molecule i, y_i is the vapor mole fraction of species i, T is the system temperature (K), and P is pressure (Pa) inside the bubble (subscript V) and in the liquid phase (subscript L). The summation is over all volatile species.

To compute the rate of loss of each volatile species, we use

$$E_{i,B} = J n_{bubble} y_i \quad (7)$$

The rate at which species i vaporizes, $E_{i,B}$ (kmol/s), is equal to the product of the rate at which bubbles nucleate, the total number of moles per bubble n_{bubble}, and the vapor mole fraction of species i. We assume that the total number of moles per bubble is constant.

Last, we assume that all bubbles that form eventually escape to the vapor phase. This seems likely when agitation is applied to a nylon-6 solution, which has a relatively low viscosity compared to PET.

Table 2. Direct-Melt Train Predictions vs Plant Data for FAV, Water Extractables, and Amine End Groups (Diffusion Only and No Mass-Transfer Limitations) at a Scaled Production Rate of 0.824[a]

polymer property	plant data	diffusion devolatilization model (surface area estimated geometrically)	no mass-transfer limitations devolatilization model
FAV	1.00	0.741	1.03
water extractables	1.00	3.73	0.651
amine end groups	1.00	1.07	0.983
		Error	
FAV error (%)		−25.9	2.65
water extractable error (%)		273	−34.9
amine end-group error (%)		7.02	−1.66

[a] The predictions and data have been scaled by the data themselves. Neither model has free parameters because the diffusion coefficient, interfacial surface area, and activity coefficients are all computed a priori.

4. Model Validation

We use Aspen Plus, Aspen Dynamics, and Polymers Plus to simulate the nylon-6 process. Polymers Plus captures polymer science and engineering fundamentals. It describes polymerization chemistries, accounts for polymer thermodynamics, and tracks polymer molecular structure using the segment-based approach.[10] Realistic simulation models of polymer manufacturing processes built using Polymers Plus and Aspen Dynamics have already begun to appear in the literature.[37−39] We implement the mass-transfer model of section 3 using the customization features available in Aspen Dynamics. We are not using the standard preprogrammed models.

4.1. Direct-Melt Process. We use a stepwise approach to predict how an industrial nylon-6 direct-melt train performs. We first consider the two limits of mass transfer: diffusion only and phase equilibrium. We then consider two alternatives to improve model predictions. One, we manually fit the interfacial surface areas for the diffusion-only model, and two, we add the boiling contribution from eq 6.

To simulate this process, we specify and solve the equations that describe each unit operation in Figure 1. We model each reactor as a series of continuous stirred-tank reactors (CSTRs), each with an equation set containing the following parts: (1) CSTR mass balance, (2) a phase-equilibrium model for front-end reactors and monomer-recovery units and a devolatilization model for back-end reactors, (3) a physical property model to compute vapor pressure and liquid density, and (4) a kinetics model for reactions in the liquid phase. We predict key process output variables of the nylon-6 that the train produces. The three characteristics are extrusion FAV, water extractables (mass %), and polymer amine end-group concentration (mmol/kg).

Table 2 shows how well the model predicts the plant data at the two limits of devolatilization. These limits are (1) diffusion only with a surface area computed geometrically (lower limit) and (2) devolatilization with no mass-transfer limitations, i.e., phase equilibrium only (upper limit). When we say "surface area computed geometrically", we mean the apparent interfacial surface area generated by the reactor internals.

The model predicts poorly in both cases. When the model predicts that too little water and caprolactam volatizes, it underpredicts the FAV (−25.9% error) and overpredicts the water extractables (273% error). On the other hand, when the model overpredicts the rate at which caprolactam volatilizes, it underpredicts the water extractables (−34.9%). Interestingly, the phase-equilibrium model correctly predicts the FAV. This shows that water experiences virtually no mass-transfer limitation in this particular direct-melt train.

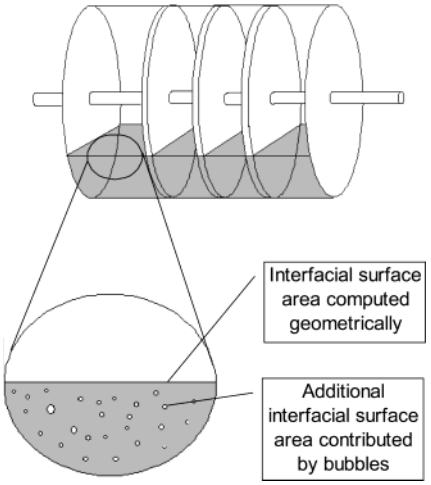

Figure 3. Vapor−liquid interfacial surface area contributions: macroscopic interfacial surface area generated by the reactor internals and microscopic interfacial surface area generated by bubbles (rotating-disk reactor shown).

One explanation as to why the diffusion-only model underpredicts the diffusion rate is that volatiles also diffuse into microscopic bubbles.[40] We do not account for this additional interfacial surface area when we estimate it geometrically. Figure 3 distinguishes between the macroscopic interfacial surface area generated by reactor internals and the microscopic interfacial surface area generated by bubbles.

The usual procedure for correcting for the presence of bubbles is to empirically increase the interfacial surface area until the model best agrees with the data.[40] By doing so, we implicitly assume that the bubble composition is equal to the reactor vapor-phase composition. We multiply the interfacial surface areas of the evaporator and finisher by 247 and 6, respectively, and predict polymer properties throughout a range of production rates. Figure 4 shows how well the model predicts the plant data for a scaled production rate range of 0.800−1.00.

We fit the evaporator surface area by using the caprolactam content in the exit polymer stream and the finisher surface area by using the hot water extractables in the extrusion stream. The justification for this is the hypothesis[40] that bubbles contribute additional surface area for diffusion. Figure 5 shows the prediction errors for the fitted diffusion model.

The fit is quite good, with average prediction errors of 2.78%, −5.59%, and −2.79% for FAV, water extractables, and amine end groups, respectively. This shows that we may not rule out the possibility that volatiles diffuse into bubbles.

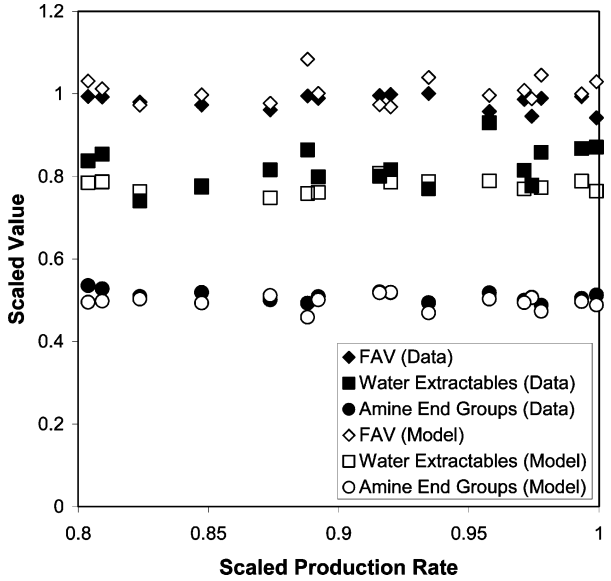

Figure 4. Direct-melt train predictions vs plant data for FAV, water extractables, and amine end groups as a function of the scaled production rate (diffusion only, with geometrically computed surface areas multiplied by 247 and 6 for the evaporator and finisher, respectively).

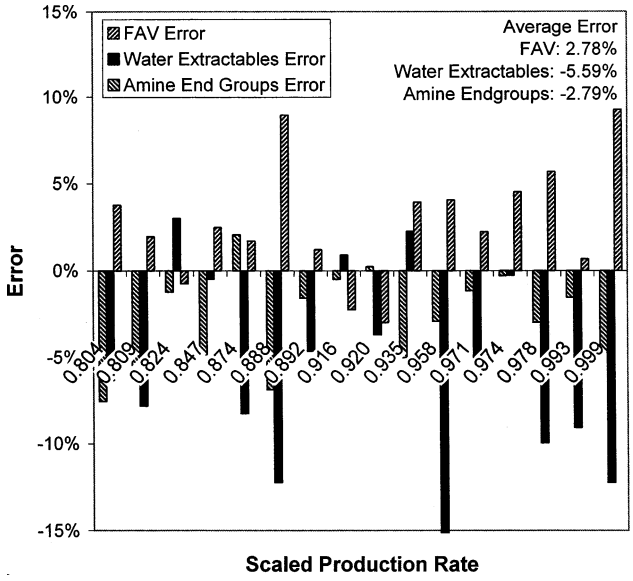

Figure 5. Direct-melt train prediction errors for FAV, water extractables, and amine end groups as a function of the scaled production rate (diffusion only, with geometrically computed surface areas multiplied by 247 and 6 for the evaporator and finisher, respectively).

However, we believe that this explanation, diffusion into bubbles with adjustments made to geometrically computed surface areas, is open to question on both conceptual and practical grounds. Traditional analysis of bubble nucleation assumes that the vapor inside of bubbles is in equilibrium with the surrounding liquid.[35] Therefore, there is no concentration driving force for mass transfer. This means that the bubbles do not contribute additional surface area for diffusional mass transfer, but rather they contribute to devolatilization simply by forming and escaping the melt phase.

The practical difficulty concerns what to do if we assume that bubbles are not in equilibrium with the liquid. Even if we could fundamentally predict the amount and size of bubbles in reactors, we would not be able to estimate the initial composition of the

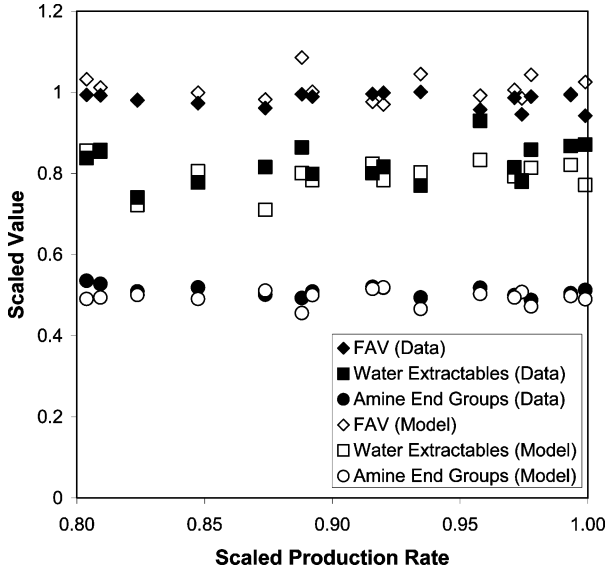

Figure 6. Direct-melt train predictions vs plant data for FAV, water extractables, and amine end groups as a function of the scaled production rate (diffusion and bubble nucleation; bubble-nucleation parameters fit to extractable data).

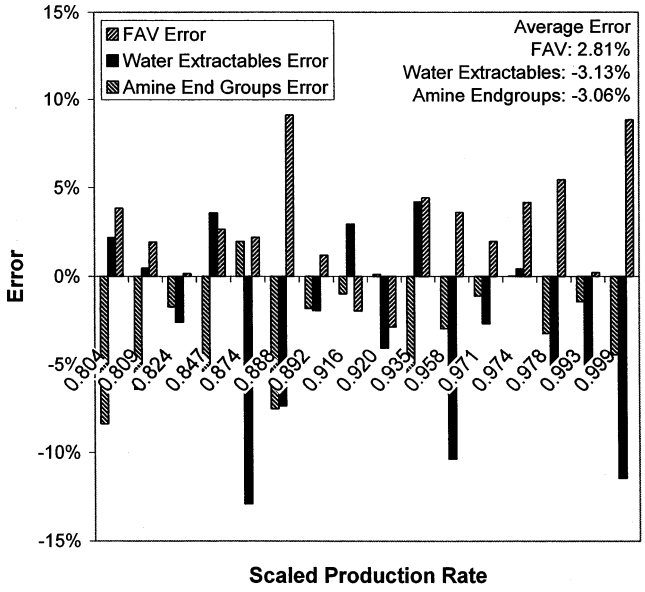

Figure 7. Direct-melt train prediction errors for FAV, water extractables, and amine end groups as a function of the scaled production rate (diffusion and bubble nucleation; bubble-nucleation parameters fit to extractable data).

bubbles. Consequently, our efforts to model polycondensation reactors degrade into mere fitting exercises that never produce a truly predictive model. This consequence alone drives us to look for alternative mechanisms for devolatilization.

We now reject the pure-diffusion hypothesis because of the above-mentioned conceptual and practical difficulties and because we have visually observed boiling in nylon-6 polymerization mixtures under vacuum. We instead assume that bubbles enhance devolatilization simply by forming and escaping the melt. We assume that this rate is described by eq 6 and fit the parameters A and B in the same way that we fit the interfacial surface area multiplication factors: by using the caprolactam content in the exit polymer stream and the hot water extractables in the extrusion stream. Figure 6 shows how well the model predicts the plant data for a

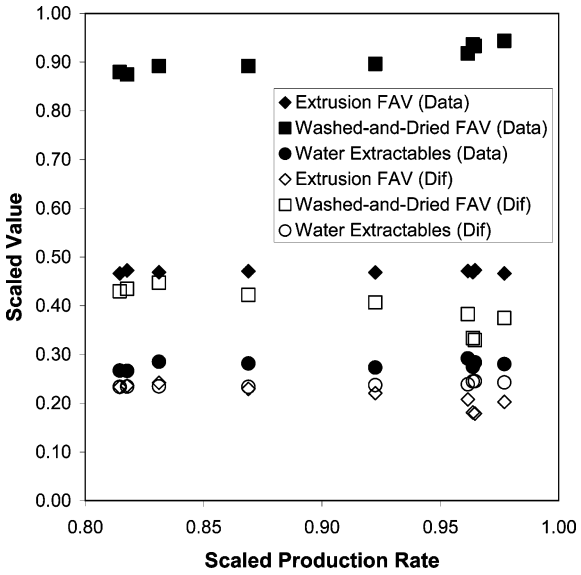

Figure 8. Bubble-gas kettle train predictions vs plant data for extrusion FAV, W&D FAV, and water extractables as a function of the scaled production rate (diffusion only; no parameter adjustments made).

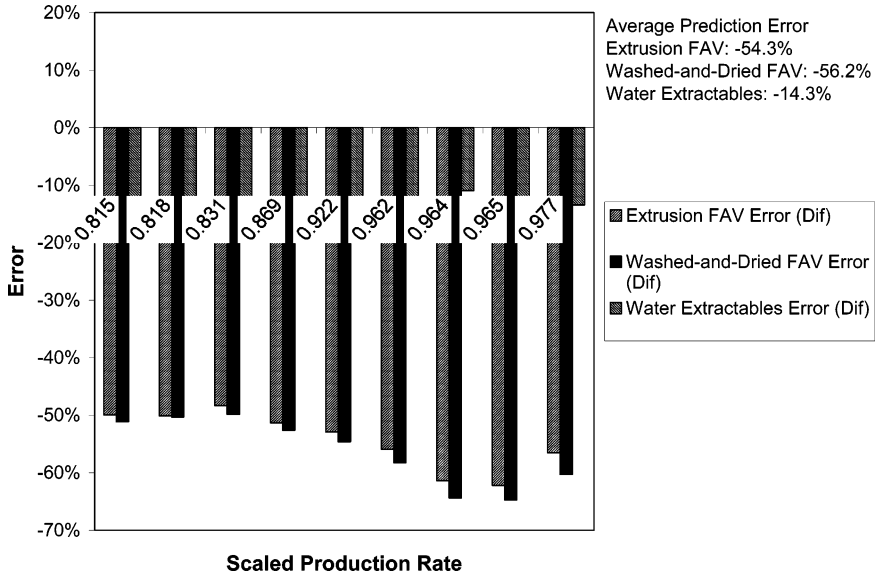

Figure 9. Bubble-gas kettle train prediction errors for extrusion FAV, W&D FAV, and water extractables as a function of the scaled production rate (diffusion only; no parameter adjustments made).

Table 3. Model Prediction Errors for the Direct-Melt Process

key process output variable error	diffusion (geometrically computed interfacial surface area)	equilibrium	diffusion (fitted interfacial surface area)	diffusion/bubble nucleation (fitted bubble-nucleation parameters)
FAV error (%)	−25.9	2.65	2.78	2.81
water extractable error (%)	273	−34.9	−5.59	−3.13
amine end-group concn error (%)	7.02	−1.66	−2.79	−3.06

range of scaled production rates. Figure 7 shows the corresponding error figures.

Like the fitted diffusion model, the combined diffusion/bubble-nucleation model is equally capable of very accurate predictions. The prediction errors are 2.81%, −3.13%, and −3.06% for FAV, water extractables, and amine end groups, respectively.

Thus far, we have discussed four models for devolatilization applied to the direct-melt train: (1) diffusion using a geometrically computed interfacial surface areas, (2) phase equilibrium only and no mass-transfer limitations, (3) diffusion using fitted interfacial surface areas, and (4) combined diffusion and bubble nucleation using fitted bubble-nucleation parameters. Table 3 shows how well the model predicts the data in each of these four cases.

The first two models predict that either too little or too much volatiles diffuse. The main conclusion of the first two analyses is that water does not experience significant mass-transfer limitations in the direct-melt process.

Both the fitted diffusion model and the fitted diffusion/bubble-nucleation model accurately predict rates at which melts devolatilize. These two models are equally capable of describing the data, but the fitted diffusion model suffers from conceptual and practical difficulties.

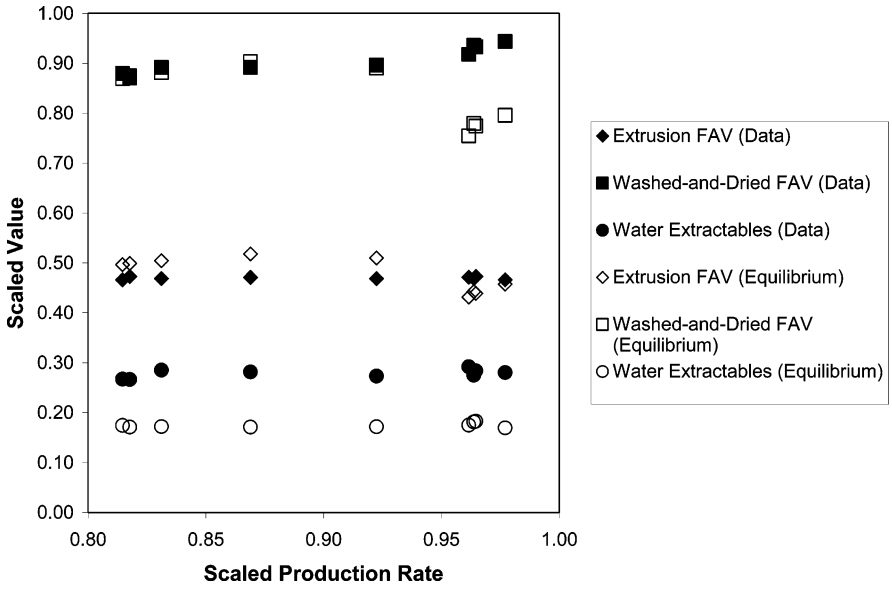

Figure 10. Bubble-gas kettle train predictions vs plant data for extrusion FAV, W&D FAV, and water extractables as a function of the scaled production rate (equilibrium; no parameter adjustments made).

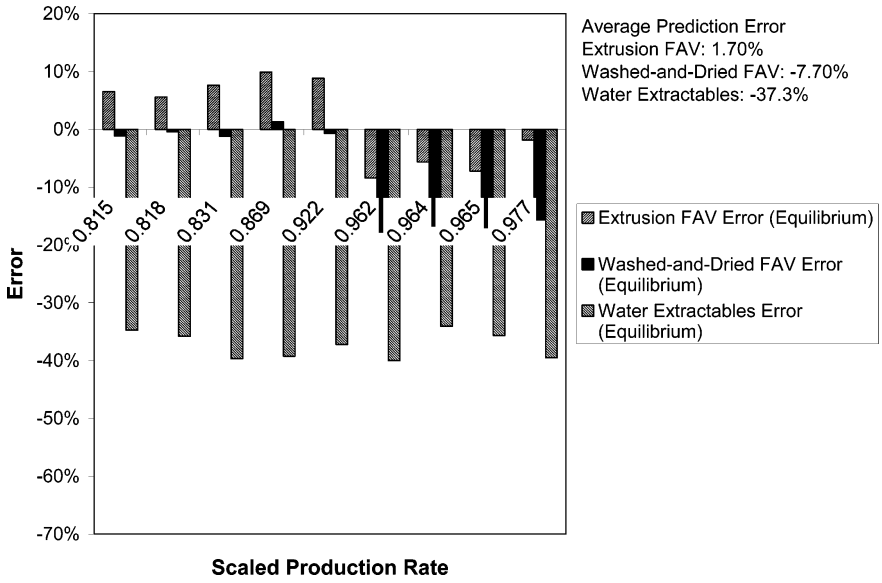

Figure 11. Bubble-gas kettle train prediction errors for extrusion FAV, W&D FAV, and water extractables as a function of the scaled production rate (equilibrium; no parameter adjustments made).

4.2. Bubble-Gas Kettle Process. Section 3 shows us how to predict, a priori, mass-transfer coefficients for forced bubbles in reactors. After our analysis in section 4.1, we can now also predict, a priori, the boiling rate as a function of the temperature, pressure, and composition. We therefore analyze the bubble-gas kettle process in a truly predictive fashion (i.e., no parameter adjustments are made) and compare how the model performs when we assume three different devolatilization cases: (1) diffusion only, (2) phase equilibrium only, and (3) diffusion and bubble nucleation.

As in the direct-melt process, we specify and solve the equations that describe the kettles in Figure 1. We model each kettle as a CSTR, with equations consisting of a mass balance, phase equilibrium in monomer-recovery units, a devolatilization model, a reaction kinetics model, and a liquid molar volume model. We predict both extrusion and W&D FAV and water extractables. Amine end groups are not measured because they can be computed from the W&D FAV as the polymer is unterminated.

Figure 8 shows how well the model predicts the plant data, assuming that melts devolatilize through diffusion only. Figure 9 shows the prediction errors.

The diffusion-only model seriously underpredicts the rate at which water volatilizes, as evidenced by the poor FAV predictions (−54.3% and −56.2% for extrusion FAV and W&D FAV, respectively). The diffusion model does, however, reasonably describe the rate at which caprolactam volatilizes, as evidenced by an underprediction of water extractables by only 14.3%. From this, we conclude that Woo et al.'s model for bubble diffusion[7−9] alone is inadequate for simulating molecular-weight growth in industrial nylon-6 bubble-gas kettle processes.

Figure 10 shows how well the model predicts plant data, assuming no mass-transfer limitations, i.e., phase equilibrium only. Figure 11 shows the corresponding prediction errors.

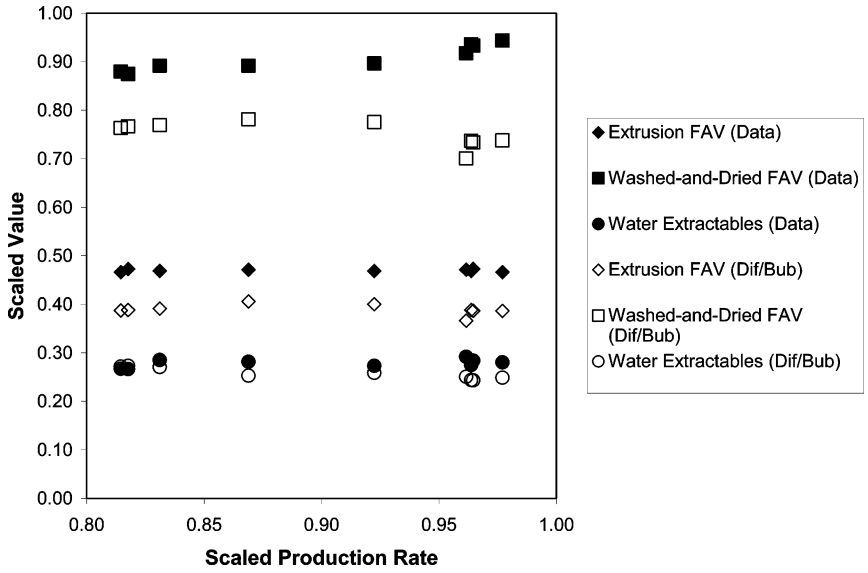

Figure 12. Bubble-gas kettle train predictions vs plant data for extrusion FAV, W&D FAV, and water extractables as a function of the scaled production rate (diffusion and bubble nucleation; no parameter adjustments made).

The prediction errors are somewhat improved over the pure-diffusion model. As in the direct-melt train, water does not appear to suffer from significant mass-transfer limitations. The equilibrium model predicts both the extrusion and W&D FAV well, with average errors of 1.70% and −7.70%, respectively. However, the equilibrium model grossly overpredicts the extent to which caprolactam volatilizes; the prediction error for water extractables is −37.3%.

An interesting aspect of the prediction error is that the phase-equilibrium model predicts well the W&D FAV at lower production rates while predicting poorly at higher production rates. We attribute this to higher sweep/forced steam flow rates. When we assume that mass-transfer limitations exist and steam is in the reactor, we would expect water to have difficulty both exiting and entering the polymer phase. When we assume phase equilibrium only, we are in danger of overpredicting the amount of water exiting and entering the polymer. We believe this to be the case here: in the higher production rates, we feed more steam to the kettles. By assuming equilibrium, the model predicts that too much water enters the polymer phase and hence too little molecular-weight growth results.

Last, Figure 12 shows how well the model predicts the plant data, assuming that both diffusion and bubble nucleation contribute to devolatilization. We believe that not including bubble nucleation, especially in considering earlier kettles where the viscosity is not high and the caprolactam content is high, is the reason for the large discrepancies seen in the diffusion-only results. Figure 13 shows the corresponding prediction errors.

The prediction errors are −17.2%, −17.0%, and −7.49% for extrusion FAV, W&D FAV, and water extractables, respectively. The model underpredicts the rate at which water volatilizes yet slightly overpredicts the rate at which caprolactam volatilizes.

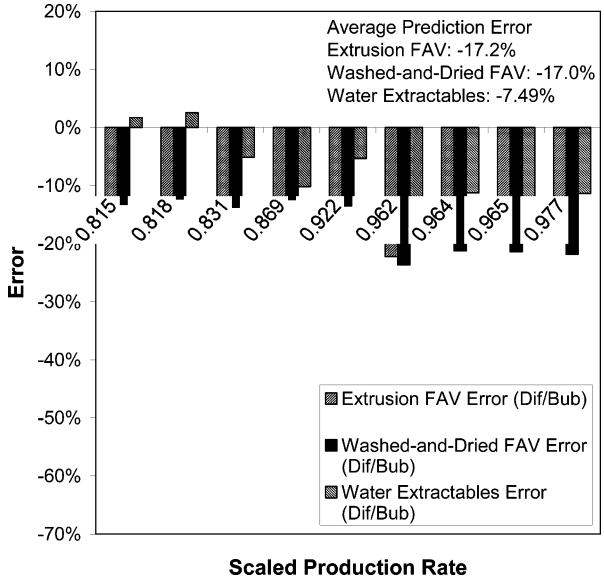

Figure 13. Bubble-gas kettle train prediction errors for extrusion FAV, W&D FAV, and water extractables as a function of the scaled production rate (diffusion and bubble nucleation; no parameter adjustments made).

To summarize, we have discussed three models for devolatilization applied to the bubble-gas kettle process: (1) diffusion using Woo et al.'s bubble dynamics model,[7−9] (2) phase equilibrium only and no mass-transfer limitations, and (3) combined diffusion and bubble nucleation using bubble-nucleation parameters

Table 4. Model Prediction Errors for the Bubble-Gas Kettle Process[a]

key process output variable error	diffusion (bubble dynamics model of Woo et al.[7−9])	equilibrium	diffusion/bubble nucleation (bubble-nucleation parameters from a direct-melt study)
extrusion FAV error (%)	−54.3	1.70	−17.2
W&D FAV error (%)	−56.2	−7.70	−17.0
water extractable error (%)	−14.3	−37.3	−7.49

[a] No parameters were fitted in obtaining these predictions.

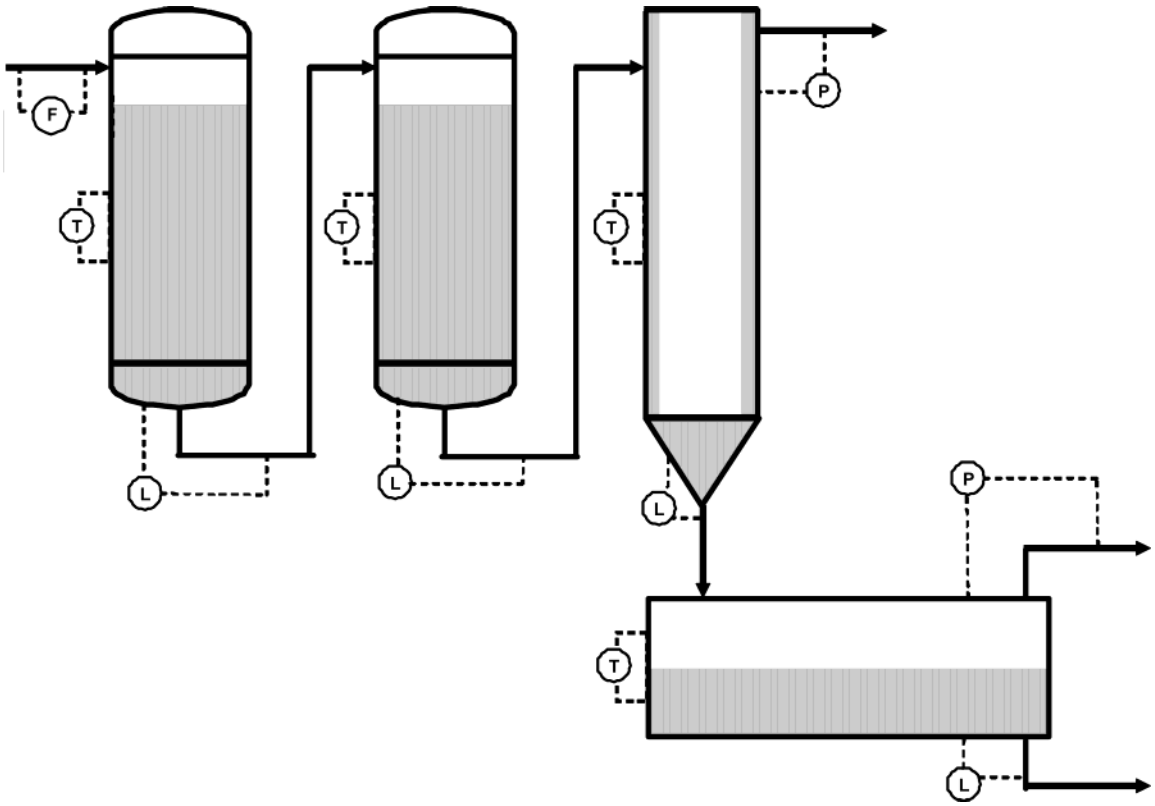

Figure 14. Simplified control scheme for the nylon-6 direct-melt process: *F*eed controllers control additive concentrations; *L*evel controllers control the liquid level by manipulating the outgoing liquid flow rate; *T*emperature controllers control the temperature by manipulating the heat duty; *P*ressure controllers control the pressure by manipulating the vapor flow rate.

from the direct-melt study. Table 4 shows how well the model predicts the data in each of these three cases.

The diffusion and equilibrium models predict that either too little or too much volatiles diffuse. Too little devolatilization leads to low FAV predictions (ca. −50% error), and too much devolatilization leads to low water extractable predictions (−37.3% error). In contrast, the diffusion/bubble-nucleation model reasonably predicts both the FAV and water extractables, with ca. 17% and −7% error, respectively.

5. Model Application

This section illustrates an application of our mass-transfer model in which we simulate a dynamic rate change in the direct-melt process. We also validate the model results by comparing model predictions with plant data. We begin by taking our steady-state model in section 4.1 and adding a control scheme. Figure 14 shows a hypothetical control scheme.

The level controllers manipulate outgoing liquid flow rates in all vessels. We control the temperature by manipulating the heat duty and control pressure in the back end by adjusting the exiting vapor flow rate. Last, additive concentrations, such as terminators and catalyst, are varied as a function of the caprolactam flow rate.

We use our dynamic model to simulate a direct-melt train, changing the relative production rate from ca. 0.98 to 0.86. Such a change is associated with decreased demand downstream of the process, e.g., shutting down fiber-spinning blocks. Figure 15 shows the profile of the relative production rate over relative time. Figure 16 shows the impact on key product qualities, as well as the pressure in the finisher.

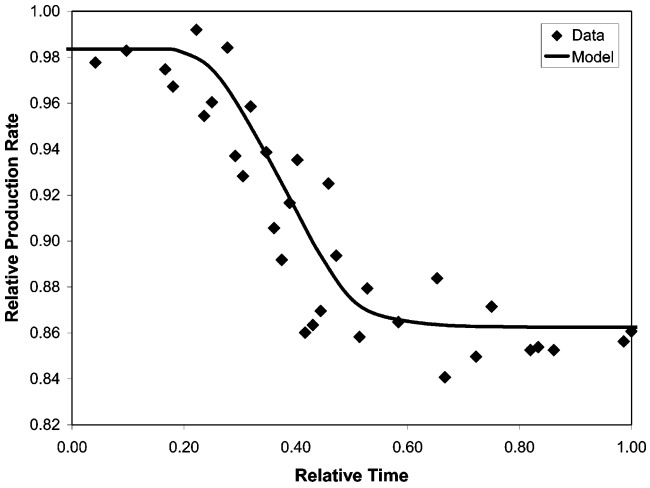

Figure 15. Production rate change in the direct-melt process.

During the initial stage of decreasing the feed rate, the viscosity in the finisher decreases. To compensate for this, the pressure controller begins to lower the pressure. The new steady-state pressure is slightly higher than the previous pressure; this is due to the increased residence time from a decrease in the rate. The product characteristics, such as water extractables, end-group concentrations, and FAV, hold relatively constant; this illustrates the robustness of the process and the associated control scheme.

6. Conclusions

In this study, we contribute a new mass-transfer model for simulating industrial nylon-6 polymerization trains. It explicitly accounts for mass transfer of vola-

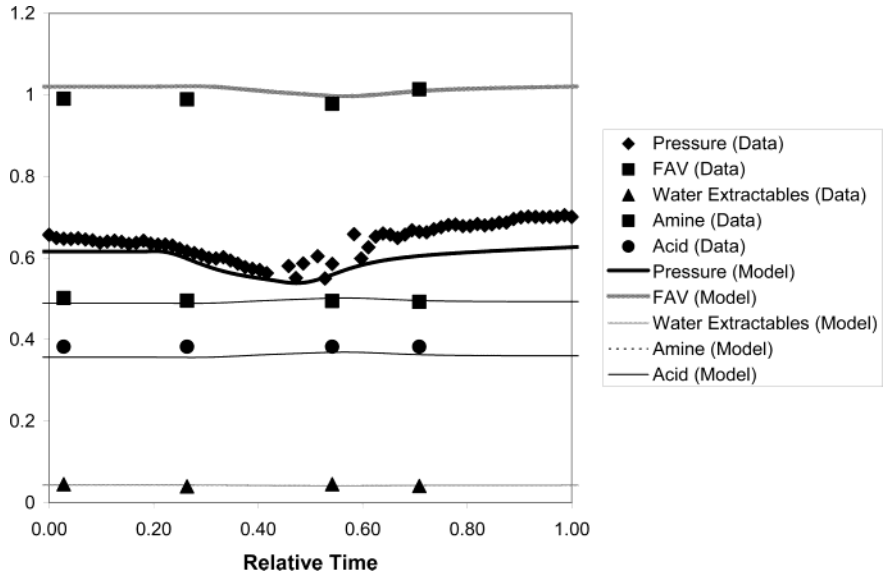

Figure 16. Product key product output variables and finisher pressure as functions of time during a rate change. All points have been normalized.

tiles through two pathways: diffusion across the liquid−vapor interface and bubble nucleation. The newness of the model comes from explicitly treating bubble nucleation, eq 6. Although it accurately approximates key features of very complicated reactors, the model is tractable and can be implemented using commercial software tools. We use this new model, with identical parameters, to accurately model two very different nylon-6 processes: the direct-melt process and the bubble-gas kettle process.

In particular, we have advanced the field of nylon-6 process modeling by showing that (i) modeling devolatilization using diffusion alone is insufficient to generate accurate predictions, (ii) to get accurate predictions using diffusion alone requires an empirical approach, with parameter adjustments being necessary for every different vessel, and (iii) including bubble nucleation allows for predictive modeling for very different processes and is the most accurate devolatilization model compared to other predictive models.

We hope to spur researchers in step-growth polymerization to more carefully consider devolatilization and consider the lessons learned in polyolefin process modeling. In particular, other researchers should study bubble nucleation rather than relying on diffusion alone to describe devolatilization.

Acknowledgment

We thank Alliant Techsystems (particularly Anthony Miano, Vice President), Aspen Technology (particularly Dustin MacNeil, Director of Worldwide University Programs, and Larry Evans, Board Chairman), China Petroleum and Chemical Corp. (particularly Xianghong Cao, Senior Vice President), Formosa Petrochemical Corp. (particularly Wilfred Wang, President), and Honeywell Specialty Materials and Honeywell International Foundation for supporting our educational programs in computer-aided design and process systems engineering at Virginia Tech. We are particularly grateful to David Tremblay, Engineering Products Business Unit, Aspen Technology, for his helpful input in this work.

Nomenclature

A_i^0 = preexponential factor for an uncatalyzed forward reaction i, kg/mol·s
A_i^c = preexponential factor for a catalyzed forward reaction i, kg^2/mol^2·s
A_{int} = interfacial area, m^2
C_i = concentration of species i in the bulk liquid phase, mol/m^3
C_{i*} = concentration of species i at the liquid-side interface, mol/m^3
d_b = bubble diameter, m
$\mathscr{D}_i$ = diffusion coefficient of species i, m^2/s
$\mathscr{D}_{i,self}$ = self-diffusion coefficient of species i, m^2/s
$\mathscr{D}_{0,i}$ = self-diffusion coefficient preexponential factor for species i, m^2/s
D_R = diameter of the reactor, m
DP_n = number-average molecular weight, kg/mol
E_i = evaporation rate for species i, mol/s
E_i^0 = activation energy for an uncatalyzed forward reaction i, J/mol
E_i^c = activation energy for a catalyzed forward reaction i, J/mol
$E_{i,B}$ = rate of species i through bubble nucleation, mol/s
$E_{i,D}$ = evaporation rate of species i through diffusion, mol/s
FAV = formic acid viscosity
g = gravitational acceleration constant, m/s^2
ΔH_i = enthalpy of reaction for reaction i, J/mol
J = nucleation rate of bubbles, #/m^3·s
k = Boltzmann's constant, J/K
K_i = equilibrium constant for reaction i
k_i = forward rate constant for reaction i, kg/mol·s
k_i' = reverse rate constant for reaction i, kg/mol·s
$k_{L,i}$ = mass-transfer coefficient for species i, m/s
M_i = molecular weight of species i
MW_w = weight-average molecular weight
n = number of moles contained in a bubble, mol
N_b = number of bubbles
P = pressure, Pa
P_e = equilibrium vapor pressure, Pa
P_i^{sat} = vapor pressure of species i, Pa
P_L = liquid pressure, Pa
P_V = pressure of gas inside a bubble, Pa
Q = volumetric flow rate, m^3/s
R = disk radius, gas-law constant, m, J/mol·K

R_i = rate equation for reaction i, mol/kg·s
S_R = cross-sectional area of the reactor, m^2
ΔS_i = entropy of reaction for reaction i, J/mol·K
T = temperature, K
u_b = bubble velocity, m/s
V_{G*} = volume per bubble, m^3
$\tilde{V}_{c,i}$ = critical molar volume of species i, m^3/mol
$\hat{V}_i^0$ = specific volume of the pure solvent, m^3/kg
V_L = reactor liquid volume, m^3
x_i = liquid-phase mole fraction of species i
y_i = vapor-phase mole fraction of species i
γ_i = activity coefficient for species i
ϵ_G = fractional gas holdup
θ = average contact time, s
μ = viscosity, Pa s
v_i = liquid molar volume of species i, m^3/mol
v_L = mixture liquid molar volume, m^3/mol
τ_{ij} = POLYNRTL binary interaction parameter for the binary $i-j$
ω = disk rotation speed, rpm

Literature Cited

(1) Yates, S. L.; Cole, C. J.; Wiesner, A. H.; Wagner, J. W. Two-Stage Hydrolysis Process for the Preparation of Nylon-6. U.S. Patent 4,310,659, 1982.

(2) Victor, L.; Saunders, J.; Rochell, D. Polymer Finisher. U.S. Patent 3,686,826, 1972.

(3) Russell, W. N.; Wiesner, A. H.; Snider, O. E. Continuous Polymerization of ϵ-Caprolactam. U.S. Patent 3,294,756, 1966.

(4) Akkapeddi, M. K.; Brown, C.; Vanbuskirk, B. Chain Extension of PA-6 and PA-6/66 Copolymer Via Reactive Extrusion with Triscaprolactamyl Phosphite (TCP). Honeywell Report, http://www.honeywell-plastics.com/literature/techpapers/0475.pdf, 3, accessed 4/2003.

(5) Seavey, K. C.; Khare, N. P.; Liu, Y. A.; Williams, T. N.; Chen, C. C. A New Phase Equilibrium Model for Simulating Industrial Nylon-6 Production Trains. *Ind. Eng. Chem. Res.* **2003**, *42*, 3900−3913.

(6) Laubriet, C.; LeCorre, B.; Choi, K. Y. Two-Phase Model for Continuous Final Stage Melt Polycondensation of Poly(ethylene terephthalate). 1. Steady-State Analysis. *Ind. Eng. Chem. Res.* **1991**, *30*, 2−12.

(7) Woo, B. G.; Choi, K. Y.; Goranov, K. The Forced Gas Sweeping Process for Semibatch Melt Polycondensation of Poly(ethylene terephthalate). *J. Appl. Polym. Sci.* **2001**, *81*, 1388−1400.

(8) Woo, B. G.; Choi, K. Y.; Song, K. H. Melt Polycondensation of Bisphenol A Polycarbonate by a Forced Gas Sweeping Process. *Ind. Eng. Chem. Res.* **2001**, *40*, 1312−1319.

(9) Woo, B. G.; Choi, K. Y.; Song, K. H. Melt Polycondensation of Bisphenol A Polycarbonate by a Forced Gas Sweeping Process. II. Continuous Rotating-Disk Reactor. *Ind. Eng. Chem. Res.* **2001**, *40*, 3459−3466.

(10) Barrera, M.; Ko, G.; Osias, M.; Ramanathan, S.; Tremblay, D. A.; Chen, C. C. Polymer Component Characterization Method and Process Simulation Apparatus. U.S. Patent 5,687,090, 1997.

(11) Gupta, S. K.; Kumar, A. *Reaction Engineering of Step Growth Polymerization*; Plenum Press: New York, 1987.

(12) Arai, Y.; Tai, K.; Teranishi, H.; Tagawa, T. Kinetics of Hydrolytic Polymerization of ϵ-Caprolactam: 3. Formation of Cyclic Dimer. *Polymer* **1981**, *22*, 273−277.

(13) ASTM Subcommittee D20.15. Standard Test Methods for Determination of Relative Viscosity and Moisture Content of Polyamide. ASTM Standard Method D 789-98, 1998.

(14) Chen, C. C. A Segment-based Local Composition Model for the Gibbs Energy of Polymer Solutions. *Fluid Phase Equilib.* **1993**, *83*, 301−312.

(15) Daubert, T. E.; Danner, R. P. *Physical and Thermodynamic Properties of Pure Chemicals. Data Compilation, Volume 3*; Hemisphere Publishing Corp.: New York, 1989.

(16) Zoller, P.; Walsh, D. J. *Standard Pressure−Volume−Temperature Data for Polymers*; Technomic: Lancaster, PA, 1995; p 278.

(17) Higbie, R. The Rate of Absorption of a Pure Gas Into a Liquid Still During Short Periods of Exposure. *Trans. AIChE* **1935**, *31*, 365−389.

(18) Ravindranath, K.; Mashelkar, R. A. Modeling of Poly(Ethylene Terephthalate) Reactors: 6. A Continuous Process for Final Stages of Polycondensation. *Polym. Eng. Sci.* **1982**, *22*, 628−636.

(19) Gupta, A.; Gupta, S. K.; Gandhi, K. S.; Mehta, M. H.; Padh, M. R.; Soni, A. V.; Ankleswaria, B. V. Modeling of Hydrolytic Polymerization in a Semibatch Nylon-6 Reactor. *Chem. Eng. Commun.* **1992**, *113*, 63−89.

(20) Gupta, S. K.; Kumar, A.; Agrawal, K. K. Simulation of Three-Stage Nylon-6 Reactors with Intermediate Mass Transfer at Finite Rates. *J. Appl. Polym. Sci.* **1982**, *27*, 3089−3101.

(21) Wajge, R. M.; Rao, S.; Gupta, S. K. Simulation of an Industrial Semibatch Nylon-6 Reactor. *Polymer* **1994**, *35*, 3722−3734.

(22) Ault, J. W.; Mellichamp, D. A. A Diffusion and Reaction Model for Simple Polycondensation. *Chem. Eng. Sci.* **1972**, *27*, 1441−1448.

(23) Gupta, S. K.; Ghosh, A. K.; Gupta, S. K.; Kumar, A. Analysis of Wiped Film Reactors Using the Orthogonal Collocation Technique. *J. Appl. Polym. Sci.* **1984**, *29*, 3217−3230.

(24) Amon, M.; Denson, C. D. Simplified Analysis of the Performance of Wiped-Film Polycondensation Reactors. *Ind. Eng. Chem. Fundam.* **1980**, *19*, 415−420.

(25) Ahn, Y. C. Effects of Diffusional Water Removal and Heat Transfer in Nylon-6 Reactors. *Polym. Eng. Sci.* **1997**, *37*, 484−493.

(26) Ravetkar, D. D.; Kale, D. D. Gas Absorption into Non-Newtonian Fluids in Rotating Disk Contactors. *Chem. Eng. Sci.* **1981**, *36*, 399−403.

(27) Nagasubramanian, K.; Reimschuessel, H. K. Diffusion of Water and Caprolactam in Nylon-6 Melts. *J. Appl. Polym. Sci.* **1973**, *17*, 1663−1677.

(28) Bonifaci, L.; Ravanetti, G. P. Measurement of Infinite Dilution Diffusion Coefficients of ϵ-Caprolactam in Nylon-6 at Elevated Temperatures by Inverse Gas Chromatography. *J. Chromatogr.* **1992**, *607*, 145−149.

(29) Zielinski, J. M.; Duda, J. L. Predictive Capabilities of a Free-Volume Theory for Polymer−Solvent Diffusion Coefficients. *Polym. Prepr. (Am. Chem. Soc., Div. Polym. Chem.)* **1991**, *32*, 394−395.

(30) Dullien, F. A. L. Predictive Equations for Self-Diffusion in Liquids: a Different Approach. *AIChE J.* **1972**, *18*, 62−70.

(31) Albalak, R. J.; Tadmor, Z.; Talmon, Y. Polymer Melt Devolatilization Mechanisms. *AIChE J.* **1990**, *36*, 1313−1320.

(32) Tukachinsky, A.; Talmon, Y.; Tadmor, Z. Foam-Enhanced Devolatilization of Polystyrene Melt in a Vented Extruder. *AIChE J.* **1994**, *40*, 670−675.

(33) Yarin, A. L.; Lastochkin, D.; Talmon, Y.; Tadmor, Z. Bubble Nucleation During Devolatilization of Polymer Melts. *AIChE J.* **1999**, *45*, 2590−2605.

(34) Gogos, C. G.; Tadmor, Z.; Kalyon, D. M.; Hold, P.; Biesenberger, J. A. Polymer Processing: An Overview. *Chem. Eng. Prog.* **1987**, *83*, 33−58.

(35) Holden, B. S.; Katz, J. L. The Homogeneous Nucleation of Bubbles in Superheated Binary Liquid Mixtures. *AIChE J.* **1978**, *24*, 260−266.

(36) Blander, M.; Katz, J. L. Bubble Nucleation in Liquids. *AIChE J.* **1975**, *21*, 833−846.

(37) Khare, N. P.; Seavey, K. C.; Liu, Y. A.; Ramanathan, S.; Lingard, S.; Chen, C. C. Steady-State and Dynamic Modeling of Commercial Slurry High-Density Polyethylene (HDPE) Processes. *Ind. Eng. Chem. Res.* **2002**, *41*, 5601−5618.

(38) Bokis, C. P.; Ramanathan, S.; Franjione, J.; Buchelli, A.; Call, M. L.; Brown, A. L. Physical Properties, Reactor Modeling, and Polymerization Kinetics in the Low-Density Polyethylene Tubular Reactor Process. *Ind. Eng. Chem. Res.* **2002**, *41*, 1017−1030.

(39) Khare, N. P.; Lucas, B.; Seavey, K. C.; Liu, Y. A.; Sirohi, A.; Ramanathan, S.; Lingard, S.; Song, Y.; Chen, C. C. Steady-State and Dynamic Modeling of Gas-Phase Polypropylene Processes Using Stirred-Bed Reactors. *Ind. Eng. Chem. Res.* **2004**, *43*, 884−900.

(40) Cheong, S. I.; Choi, K. Y. Melt Polycondensation of Poly(ethylene terephthalate) in a Rotating Disk Reactor. *J. Appl. Polym. Sci.* **1995**, *58*, 1473−1483.

Received for review February 23, 2004
Revised manuscript received May 21, 2004
Accepted May 25, 2004

IE040067L